1977SSRv...21..259B

THE PLASMA EXPERIMENT ON THE 1977 VOYAGER MISSION

H. S. BRIDGE, J. W. BELCHER, R. J. BUTLER, A. J. LAZARUS, A. M. MAVRETIC, and J. D. SULLIVAN

Center for Space Research and Physics Department, Massachusetts Institute of Technology, Cambridge, Mass. 02139, U.S.A.

and

G. L. SISCOE

Department of Meteorology, University of California, Los Angeles, Calif., U.S.A.

and

V. M. VASYLIUNAS

Max-Planck-Institut Für Aeronomie, Katlenburg-Lindau, F.R.G.

(Received 24 May 1977)

Abstract. This paper contains a brief description of the plasma experiment to be flown on the 1977 Voyager Mission, its principal scientific objectives, and the expected results.

The instrument consists of two Faraday cup plasma detectors: one pointed along and one at right angles to the Earth-spacecraft line. The Earth-pointing detector uses a novel geometrical arrangement: it consists of three Faraday cups, each of which views a different direction in velocity space. With this detector, accurate values of plasma parameters (velocity, density, and pressure) can be obtained for plasma conditions expected between 1 and 20 AU. The energy range for protons and for electrons is from 10 to 5950 eV. Two sequential energy per charge scans are employed with nominal values of $\Delta E/E$ equal to 29%, and 3.6%. The two scans allow the instrument to cover a broad range between subsonic ($M < 1$) and highly supersonic ($M \simeq 100$) flows; thus, significant measurements can be made in a hot planetary magnetosheath as well as in a cold solar wind. In addition, the use of two energy resolutions during the cruise phase of the mission allows simultaneously the measurement of solar wind properties and a search for interstellar ions.

The Earth-pointing detector cluster has an approximately conical field of view with a half angle of 90°. The exceptionally large field of view makes this detector especially suited for use on a three-axis stabilized spacecraft. Both the solar wind direction during the cruise phase of the mission, and the deviated magnetosheath flow directions expected at Jupiter and Saturn fall within the field of view of the main detector; thus, no mechanical or electrical scanning is required. An additional sensor with a field of view perpendicular to that of the main cluster, is included to improve the spatial coverage for the drifting or corotating positive ions expected at planetary encounter. This detector is also used to make measurements of electrons in the energy range 10 to 5950 eV.

The scientific goals include studies of (a) the properties and radial evolution of the solar wind, (b) the interaction of the solar wind with Jupiter, (c) the sources, properties and morphology of the Jovian magnetospheric plasma, (d) the interaction of magnetospheric plasma with the Galilean satellites with particular emphasis on plasma properties in the vicinity of Io, (e) the interaction of the solar wind with Saturn and the Saturnian satellites with particular emphasis on Titan, and (f) ions of interstellar origin.

1. Experimental Requirements

The Voyager plasma instrument has been designed to meet five main requirements imposed by spacecraft constraints, the expected Jovian environment, and the

Space Science Reviews **21** (1977) 259–287. *All Rights Reserved*
Copyright © 1977 by D. Reidel Publishing Company, Dordrecht-Holland

© Kluwer Academic Publishers • Provided by the NASA Astrophysics Data System

1977SSRv...21..259B

scientific objectives discussed below in Section 4:

(1) The instrument must measure plasma properties in the solar wind and at planetary encounters for a wide range of flow angles. Since the Voyager spacecraft is stabilized about three axes, no angular scan is provided by the spacecraft itself and the problem of measuring flow speeds, flow angles, temperatures, and densities over the expected range of these parameters is particularly severe.

(2) The experiment must operate properly in the Jovian charged particle environment.

(3) The instrument must cover a wide energy range with adequate sensitivity and resolution to measure the low particle densities and to resolve the very narrow energy and angular distributions which occur in the solar wind at large distances, but it must also be able to observe the broad angular and energy distributions and the large deviations of flow direction expected in the magnetosheaths and magnetospheres of Jupiter and Saturn. In addition, the instrument must detect and measure the broad distributions of ions which are 'picked up' by the solar wind from ionization of neutral atoms from the interstellar gas or from planetary atmospheres.

(4) The instrument should be able to measure the properties of the corotating low energy plasma expected to be present in the inner Jovian magnetosphere.

(5) For the solar wind or magnetosheath plasma, the instrument should provide the velocity space moments of the particle distribution function (i.e., the macroscopic plasma parameters) via a simple and direct three-dimensional analysis.

2. Experiment Description

2.1. Sensor design and operation

The instrument which was developed to satisfy these requirements is an adaptation and extension of the modulated Faraday cup plasma detector (Bridge *et al.*, 1960; Vasyliunas, 1971; Bridge and Vasyliunas, 1973). The instrument consists of two plasma detectors; one, the $-Z$ detector, points toward the Earth and roughly into the solar wind flow. The other, the lateral detector, points approximately into the corotating flow during the inbound trajectory at Jupiter encounter. A photograph of the instrument is shown in Figure 1.

A conventional Faraday cup consists of a collector, several grids and one or more apertures which define the field of view for the incident plasma flux. Usually the collector and grids lie in parallel planes. A composite dc–ac waveform is applied to one of the grids, the modulator grid, and this retarding potential selects incident ions in a corresponding energy per charge interval. The collector can be a single plate or it may be split into two or more segments; in the latter case, the relative currents to the segments give information about the direction of plasma flow relative to the symmetry axis of the sensor.

The lateral sensor is of the conventional type; it contains a single collector plate and eight grids. Six of the grids are used as electrostatic shields and/or to suppress

© Kluwer Academic Publishers • Provided by the NASA Astrophysics Data System

1977SSRv...21..259B

secondary electrons and the remaining two serve respectively to select the energy per charge range for positive or negative ions. For positive ions a positive potential is applied to the first of the two modulator grids while the second is held at ground potential; for electrons or negative ions the first modulator grid is held at ground and a negative potential is applied to the second modulator grid.

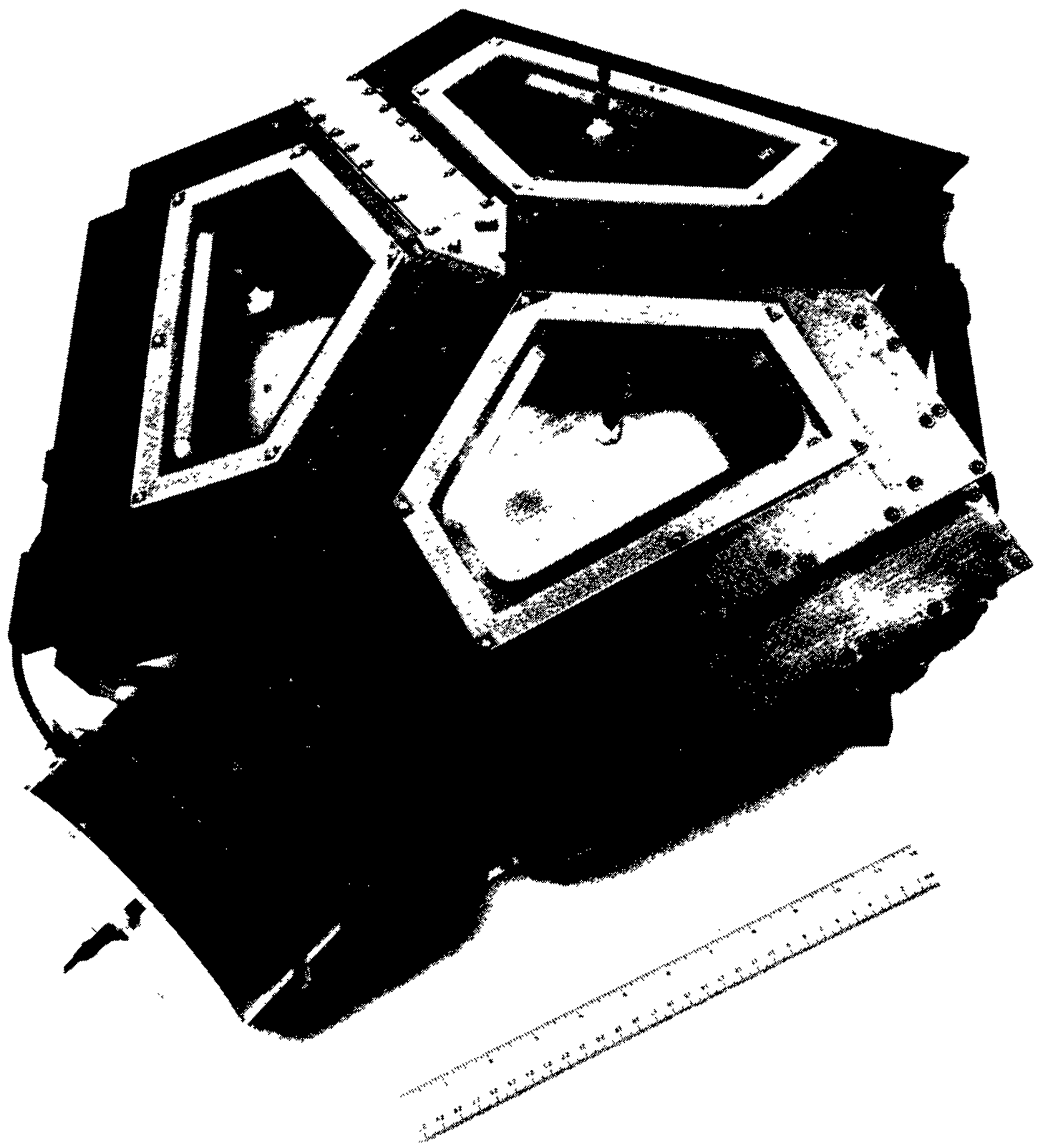

Fig. 1. Photograph of the Voyager plasma instrument. The three apertures of the main sensor are visible; the lateral detector is in the lower left region of the view. The axis of symmetry of the main sensor cluster is directed parallel to the $-Z$ axis of the spacecraft (the Earth-pointing direction). In this photograph the apertures of the sensors are closed by protective covers which are removed before launch; each cover is fitted with a connection for a purge gas.

© Kluwer Academic Publishers • Provided by the NASA Astrophysics Data System

1977SSRv...21..259B

In contrast to the lateral detector, the Earth-pointing detector uses a novel geometrical arrangement of three Faraday cup sensors to determine the macroscopic properties of the plasma ions. Consider a flat surface of the spacecraft normal to the $-Z$ axis. Sitting on this surface are three collector plates that form three faces of a tetrahedron each at 20° to the $-Z$ axis; above them is the usual set of parallel grids – suppressor, shields, and modulator – but each grid is again three faces of a tetrahedron, similar to the set of collectors; and finally, there is the outer surface which is a tetrahedron with an aperture cut into each face. A photograph of the structure is shown in Figure 1, and a schematic cross-sectional view through one face of the tetrahedral structure is shown in Figure 2. (Note that in the actual instrument it proved advantageous to cut out some parts of the tetrahedron.)

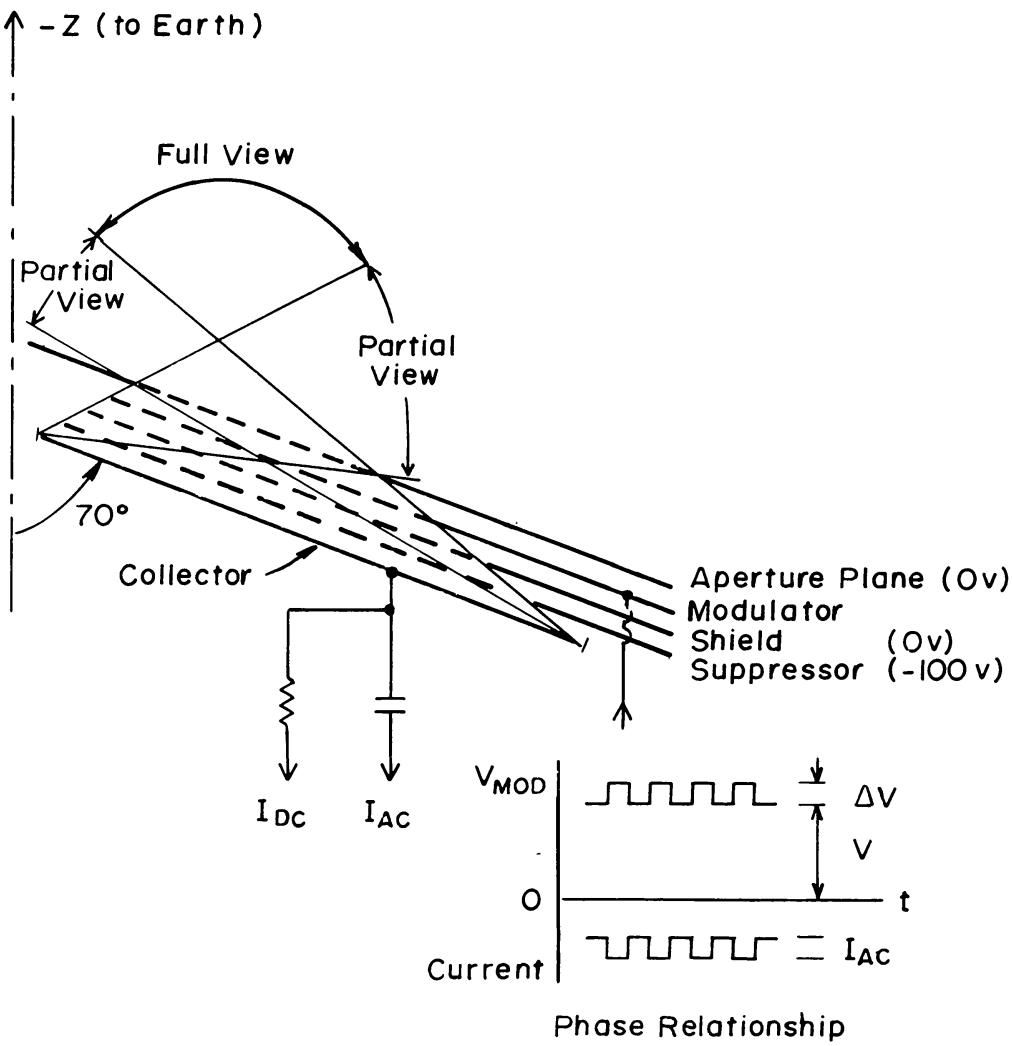

Fig. 2. A cross sectional view of the grid structure (schematic) for one of the three sensors of the $-Z$ detector. For clarity only a single shield grid and a single modulator grid are shown. In the actual sensor six shield grids are used to obtain sufficient electrical isolation between the modulator and collector, and three grids are used for the modulator so that the retarding potential is defined to 0.5%.

© Kluwer Academic Publishers • Provided by the NASA Astrophysics Data System

1977SSRv...21..259B

An essential feature of the design is that the structure is very shallow. This has the result (see Figures 1, 2, and 3) that there is a wide range of directions from which incident particles can traverse an aperture and reach the collector plate unobscured by anything except the grids (which are very transparent and have a small effect). The full field of view of an individual sensor is the angular range for which (neglecting the opacity of the grid structure) all particles incident on the aperture reach the collector. These full view directions lie within a noncircular cone whose axis is normal to the collector. For angles of incidence outside the full field, the image of the aperture moves off the collector and only part of the plasma incident on the aperture is

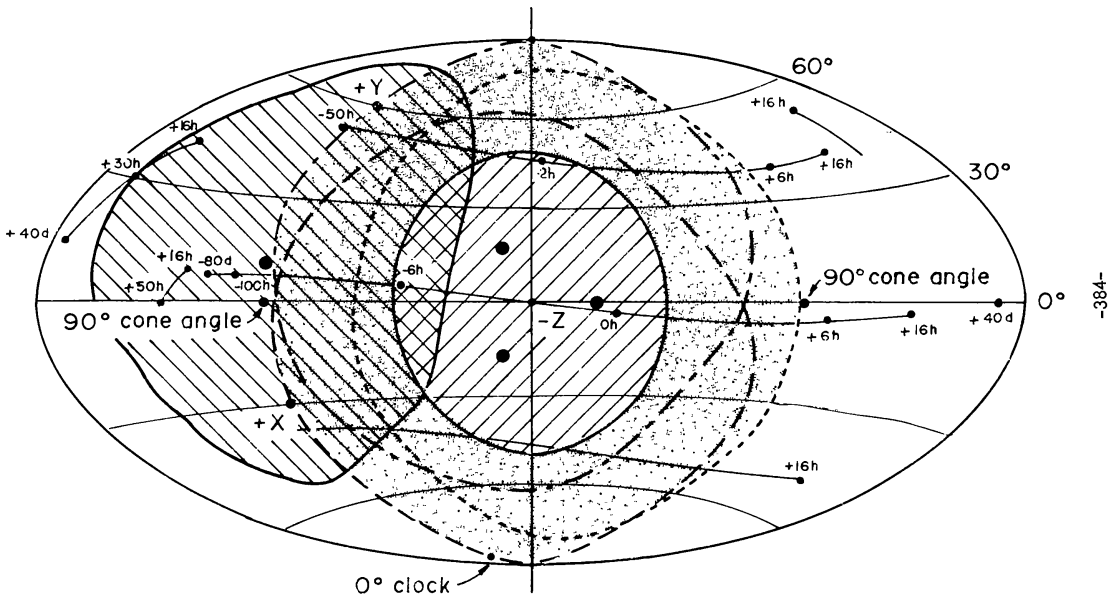

Fig. 3. The fields of view of the four plasma sensors projected onto an all sky map. The origin of the coordinate system is the $-Z$ axis of the spacecraft; the $+X$ and $+Y$ axes are also shown, and the position of 0° 'clock angle' defined by the Canopus star tracker is indicated. The four large dots represent the directions of the normals of the four sensors. The three dots closest to the origin are the three view directions of the $-Z$ detector, and the dashed lines show the limits of the partial view cones of these sensors. Similarly, the solid closed curve to the left of the origin shows the partial view cone for the lateral sensor. The central circular area consists of the three full view cones of the $-Z$ detector; it defines the primary field of view used for solar wind measurements. The dotted area is the secondary field for the $-Z$ detector. In a magnetosheath or magnetosphere the useful field of view is defined by the combined partial view cones for all four sensors.

During Jupiter encounter ions from the ionosphere are expected to travel north and south along the field lines whereas ions from the Jovian satellites should corotate with the field and be confined to a region near the equatorial plane (see Section 4.3). The arrival directions of these ions during the JST encounter are shown primarily by the three nearly horizontal lines in the figure. Times on those lines are in hours, h, or days, d; negative times indicate times before encounter. The corotating satellite ions are indicated by the line near the equator which begins at its left end at −80 days, continues to the right until +16 hours at which time the spacecraft rolls ~125° and those ions appear near the left edge of the figure at approximately 45°N latitude. Ionospheric ions traveling towards the south ecliptic appear first at the left end of the upper angular position line (≃40°N latitude) at −50 hours; their angular position moves to the right until +16 hours; after the roll, they appear at the upper right edge of the figure. Northward moving ions are indicated by the remaining lines.

© Kluwer Academic Publishers • Provided by the NASA Astrophysics Data System

1977SSRv...21..259B

measured. Directions in this region are called partial view directions. The partial view directions for the three sensors of the Earth-pointing detector are shown in Figure 3. The three heavy dots near the center of the figure represent the directions normal to the three collectors of the instrument and the dashed lines bound the partial view directions. The shaded area consists of the directions common to all three *full* view cones; we call this region the 'primary' field of view. It is approximately a cone of half-angle 45°. For most of the mission practically all the solar wind ions will be within the primary field of view, and this is also true of magnetosheath ions for many of the flow conditions that may be encountered. Outside the primary field of view lies the secondary field of view; in this region plasma can still be seen but not all the particles which pass through a given aperture reach the corresponding collector (see Figure 2); this region is contained in a cone of half-angle 90°, so it includes a complete hemisphere. The field of view of the lateral detector is also shown in Figure 3.

As discussed in detail in Section 3 below, this geometrical arrangement permits a direct determination of the moments of the solar wind distribution function.

2.2. Electronics Design and Data Acquisition

The simplified block diagram in Figure 4 illustrates the approach taken in the design of this instrument. Currents from three collectors (A, B, and C) of the $-Z$ detector and that from the lateral sensor (collector D) are amplified, filtered and integrated

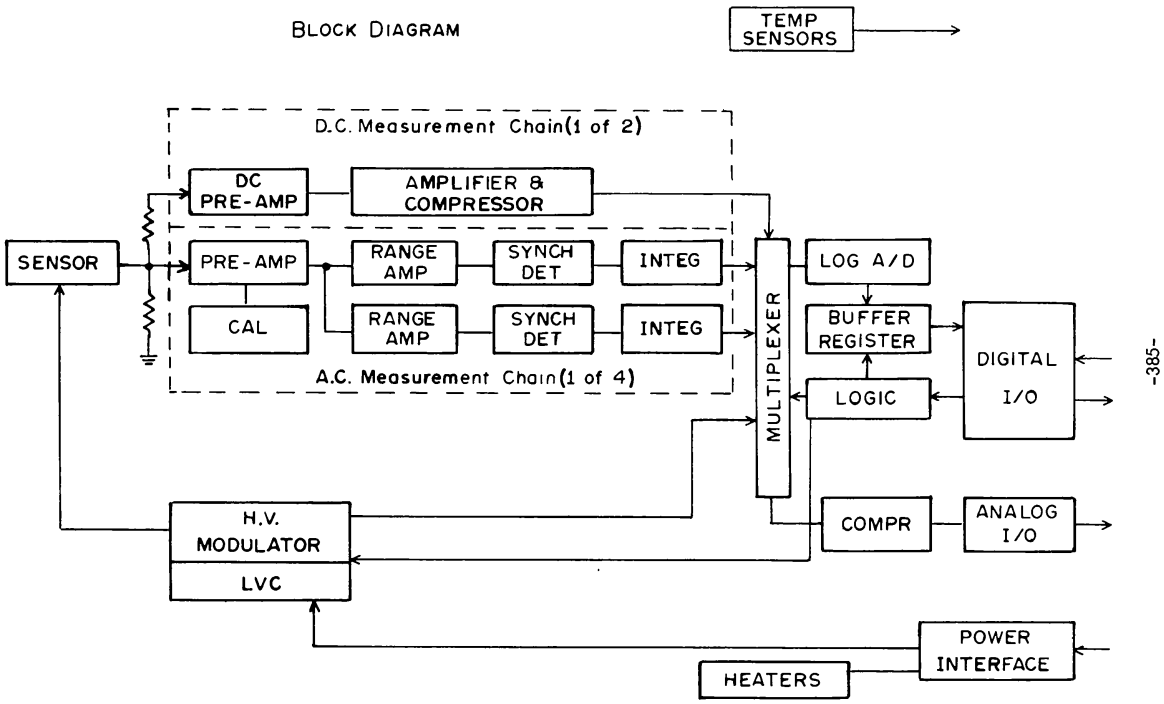

Fig. 4. Block diagram of the Voyager plasma instrument for one of the four sensors. The dc measurement chains measure the total positive or negative currents to the collector of one sensor in the $-Z$ detector and to the collector of the lateral detector.

© Kluwer Academic Publishers • Provided by the NASA Astrophysics Data System

1977SSRv...21..259B

using four separate measurement chains. A single 8-bit logarithmic A to D converter samples the four outputs of the measurement chains and transfers the data to the spacecraft through the data/timing interface. Selected critical power supply voltages and internal temperatures are transmitted via the engineering telemetry data stream.

The high voltage modulator supplies a dc pedestal and a superimposed 400 Hz square wave modulation voltage. For positive ions the modulator grids of all four sensors are driven in parallel and two sequential energy per charge scans are used over the range 10 to 5950 V. The voltage windows are contiguous and to first order increase in width logarithmically as the voltage level increases. The low resolution mode (the L mode) consists of 16 steps with $\Delta E/E \geqslant 0.29$; the high resolution mode (the M mode) consists of 128 steps with $\Delta E/E \geqslant 0.036$. For electrons a negative waveform is applied to a different modulator grid in the lateral sensor. A sixteen-step scan (the E_1 mode) with $\Delta E/E \geqslant 0.099$ covers the energy range 10 to 140 eV and is used to measure solar wind electrons; a second sixteen-step scan (the E_2 mode) with $\Delta E/E \geqslant 0.29$ covers the energy range 10 to 5950 eV and is used at planetary encounters to measure magnetospheric electrons. The Earth-pointing detector is not used during the electron scans. Table I gives a summary of the instrument characteristics.

Figure 4 also shows details of the measurement chain design: the high input impedance, low noise linear preamplifier converts the collector current to a voltage over a range of more than six decades. Its low impedance output drives two range amplifiers, one of which has a gain 100 times the other. Each range amplifier drives an independent integrator through a demodulator in phase synchronism with the modulated 400 Hz signal. If the integrator associated with the higher gain amplifier is saturated, the most significant bit (MSB) of the 8-bit output word is set to 1 and the voltage on the other integrator is logarithmically converted to a 7-bit word. If the integrator associated with the higher gain amplifier is not saturated, then the MSB is set to 0 and its output is converted. In-flight calibrations of each measurement chain and of the complete range of modulator voltages are subcommutated into the data flow by the formatting and timing logic.

The sensitivity of the instrument depends on the signal-to-noise ratio which can be achieved and is limited mainly by Johnson noise in the input resistor; the signal-to-noise ratio is, of course, a function of integration time. Early in the mission, sensitivity is not a problem and nominal integration times of 30 and 210 millisec are used; later in the mission (beyond about 10 AU) maximum sensitivity is required and an integration time of 930 millisec is used for each current sample. Table II contains a summary of the possible operating modes of the instrument during the mission. The exact choice of mode depends on the performance of the telemetry link and on the sensitivity which is required. Note that the minimum cycle time, i.e., the time to obtain complete positive ion and electron spectra is 12 sec for the 30 millisec integration time; the maximum cycle time (930 millisec integration time) is 192 sec in Cruise 6 and 384 sec in Slow Cruise. Corresponding bit rates range from 200 to 8 bps. Within the Jovian magnetosphere we expect that the sensitivity of the

© Kluwer Academic Publishers • Provided by the NASA Astrophysics Data System

1977SSRv...21..259B

TABLE I

Summary of instrument characteristics

Energy and velocity range

Ion	Mode	Energy (eV)	Velocity[a] (km sec^{-1})
H^+	M/L	10–5950	44–1069
He^{++}	M/L	20–11900	31–756
Na^+	M/L	10–5950	9.2–223
S^+	M/L	10–5950	7.7–189
e^-	E_1	10–140	$(1.89–7.1)\times10^3$
e^-	E_2	10–5950	$(1.89–45.8)\times10^3$

Energy/charge scan

Mode	Resolution[b] ($\Delta E/\bar{E}$)	k	Steps	Detector
M	0.20–0.036	1.03663	128	$-Z$ and lateral
L	1.00–0.29	1.33352	16	$-Z$ and lateral
E_1	0.37–0.099	1.07461	16	lateral
E_2	1.00–0.29	1.33352	16	lateral

Resolution and accuracy[c]

Angular	Density	Velocity	Thermal speed	Notes
0.15° relative	3% relative	1% relative	10% relative	For Mach number
0.3°	10% absolute	5% absolute	15% absolute	$30>M>3$

Sensitivity

	Effective collector area[d] (cm^2)	Solid angle (ster)	Geometrical factor (cm^2 ster)	Minimum measurable directed flux (cm^{-2} sec^{-1})[e]	Minimum measurable isotropic flux (cm^{-2} sec^{-1} ster^{-1})[f]
$-Z$ Detector (cluster)		0.6π		$\leq 6\times10^3$	
$-Z$ Detector (each sensor)	65	π	200	3×10^3	1.0×10^3
Lateral detector	65	π	125	3×10^3	1.6×10^3

Electrical and physical characteristics

Cycle time (sec)	ac Amplifier noise limit (amp)	ac Amplifier dynamic range	dc Amplifier sensitivity/range (amp)	Weight (kg)	Power (watts)
384	3×10^{-14}	2×10^6	$\pm(10^{-10}$ to $10^{-7})$	9.9	8.1
192	3×10^{-14}				
96	6×10^{-14}				
12	2×10^{-13}				

© Kluwer Academic Publishers • Provided by the NASA Astrophysics Data System

1977SSRv...21..259B

Notes for Table I

[a] Velocities given are for normal incidence on the detector; for angles of incidence of 30° to the detector normal, values are approximately 15% higher.

[b] The *nominal* dc retarding potentials applied to the modulator increase logarithmically as $V = V_0 k^{n-1}$, where n is the step number and $V_0 = 60$ volts. The associated ac waveform, ΔV_n, increases so that the energy windows are contiguous: i.e., $\Delta V_n = V_0(k-1)k^{n-1}$. Thus, nominally, $\Delta V_n / V_n$ would be $(k-1)$. To detect very low energy ions, we wanted V_1 to be 10 volts instead of the nominal value of 60 volts. To maintain the same dynamic range for the modulator control system, a constant bias of 50 volts was subtracted from all dc levels. Thus the *actual* values of $\Delta V/V$ become close to the nominal value for dc retarding potentials of greater than a few hundred volts.

[c] As discussed in Section 3, the relative accuracies depend strongly on the Mach number and number density. See the discussion and Table III of Section 3. The values quoted here are for typical conditions expected at 20 AU. The absolute errors represent a subjective estimate of systematic errors.

[d] Includes the effect of grid transparency.

[e] For solar wind measurements using data from the three sensors in the $-Z$ detector.

[f] Assumes all flux in a single energy/charge channel.

instrument will be limited by background effects produced by the Jovian radiation belts. In particular, high energy particles which penetrate the input field-effect transistors produce additional carriers and hence an increase in the direct current which flows in the preamplifier input. Fluctuations in this current produce an increase in the noise current at the input of the preamplifier. The effect varies as the square root of the radiation flux and can be reduced by shielding the input transistors. These devices were shielded with about 8 gm cm^{-2} of copper so that at the orbit of Io, we expect to be able to measure an input signal current of 10^{-13} amp. At 10 R_J, the effect of the Jovian charged particle radiation can be neglected, and the current sensitivity is $\simeq 5 \times 10^{-14}$ amp.

3. Calculation of Plasma Parameters

The basic experimental data are the modulated components of the currents to the three collectors for a sequence of contiguous energy windows defined by the modulator waveform. If $\hat{n}$ is the unit vector normal to a given collector, and the modulator potential varies between Φ_1 and Φ_2 for the kth energy window, then the modulated current I_k is related to the particle velocity distribution function $f(\mathbf{v})$ by the following integral:

$$I_k = eA \int \mathrm{d}^3 v f(\mathbf{v}) \mathbf{v} \cdot \hat{n} G(\mathbf{v}, \hat{n}) W_k(\mathbf{v} \cdot \hat{n}) , \tag{1}$$

where A is the area of the entrance aperture, G is the fraction of the aperture that intercepts the collector when projected at a given direction of incidence. W_k describes the energy window:

$$\begin{aligned} W_k &= 0, & \mathbf{v} \cdot \hat{n} &< u_1; \\ &= 1; & u_1 < \mathbf{v} \cdot \hat{n} &< u_2; \\ &= 0, & u_2 &< \mathbf{v} \cdot \hat{n}; \end{aligned}$$

© Kluwer Academic Publishers • Provided by the NASA Astrophysics Data System

1977SSRv...21..259B

TABLE II
Sequence definition

SEQUENCE DEFINITION

SEQUENCE	TEL. RATE BITS/SEC	SEQUENCE TIME SEC	PLS BITS/SEC	MODES IN SEQUENCE	SAMPLE CLOCK SEC	MEASUREMENT PERIOD SEC	TIME TO NEXT MODE SEC	CUP DATA TO FDS	CUP DATA TELEMETERED	# WORDS TELEMETERED	REMARKS
Encounter (Standard)	3600	96	32	M	.240	30.72	6.72	ABCD	ABCD	4x72	
				E_1		3.84	20.16	ABCD	D	16	FDS alternately selects first 72 word or last 22 word subset of M mode data on successive sequences
				L		3.84	20.16	ABCD	ABCD	4x16	
				E_2		3.84	6.72	ABCD	D	16	
Cruise 1	2560	12	202.67	M	.060	7.68	1.68	ABCD	ABC	3x96	FDS selects last 96 word subset of M mode data or alternates between first 96 word and last 96 word subset on successive spectra by command
				E_1		0.96	1.68	ABCD	D	16	
Cruise 2	1280	96	32	M	.240	30.72	6.72	ABCD	ABC	3x96	
				E_1		3.84	20.16	ABCD	D	16	Same as Cruise 1
				L		3.84	20.16	ABCD	ABCD	4x16	
				E_2		3.84	6.72	ABCD	D	16	
Cruise 3/4	640/320	96	32	M	.240	30.72	6.72	ABCD	ABC	3x96	
				E_1		3.84	20.16	ABCD	D	16	Same as Cruise 1
				L		3.84	20.16	ABCD	ABCD	4x16	
				E_2		3.84	6.72	ABCD	D	16	

© Kluwer Academic Publishers • Provided by the NASA Astrophysics Data System

1977SSRv...21..259B

TABLE II (*cont.*)

Cruise 5 & 6A	160	192	16	M	.240	30.72	30.72	ABCD	ABC	3x96	Same as Cruise 1
				E_1		3.84	44.16	ABCD	D	16	
				L		3.84	44.16	ABCD	ABCD	4x16	
				E_2		3.84	30.72	ABCD	D	16	
Cruise 6 (Saturn)	80	192	16	M	.960	122.88	5.76	ABCD	ABC	3x96	Same as Cruise 1
				E_1		15.36	5.76	ABCD	D	16	
				L		15.36	5.76	ABCD	ABCD	4x16	
				E_2		15.36	5.76	ABCD	D	16	
Cruise (Slow)	40	384	8	M	.960	122.88	26.88	ABCD	ABC	3x96	Same as Cruise 1
				E_1		15.36	80.64	ABCD	D	16	
				L		15.36	80.64	ABCD	ABCD	4x16	
				E_2		15.36	26.88	ABCD	D	16	

© Kluwer Academic Publishers • Provided by the NASA Astrophysics Data System

1977SSRv...21..259B

where $e\Phi \equiv \frac{1}{2}mu_1^2$, $e\Phi_2 \equiv \frac{1}{2}mu_2^2$; e and m are the charge and the mass of the ions. Equation (1) should be summed over all the positive ion species present in the plasma; in the solar wind, however, the energy spectra are expected to be sufficiently narrow so that currents due to protons and to alpha particles can be distinguished* and the analysis described below can be carried out separately for the two species.

The essential features of the instrument are (1) by virtue of the geometrical design, the angular response function G is unity** for all directions lying within the primary field of view, i.e., all particles incident on the defining aperture reach the collector; and (2) the width of the energy window is small compared to the width of the particle energy spectrum (thus the function W_k can be approximated by a Dirac delta function). Therefore, as long as the plasma is within the primary field of view, Equation (1) can be approximated as:

$$I_k \approx eA\,\Delta u_k \int \mathrm{d}^3v f(\mathbf{v})\mathbf{v}\cdot\hat{n}\delta(u_k - \mathbf{v}\cdot\hat{n})\,, \tag{2}$$

where

$$\Delta u_k \equiv u_2 - u_1 \quad \text{and} \quad u_k \equiv \tfrac{1}{2}(u_2 + u_1)\,.$$

Thus, as long as the plasma ions lie within the primary field of view, the current to any collector is proportional to the integral of the distribution function over a plane in velocity space that is parallel to the collector. This is the key to the computation of the moments of the distribution.

A technique which is sometimes called the method of moments is used to compute the plasma parameters from the measured currents. While ordinarily this method gives rather approximate results, we shall show that, as a result of the unique properties of the present instrument that lead to Equation (2), the method of moments yields the actual values of the macroscopic plasma parameters and does not require the introduction of a particular form for the plasma velocity distribution function. We form the sum of the measured currents from a given collector, weighted by a power ν of the speed corresponding to the center of each energy window:

$$M_\nu \equiv \sum_k \frac{I_k}{eA\,\Delta u_k} u_k^\nu \Delta u_k\,. \tag{3}$$

Under the same approximations as for Equation (2), the sum is equal to the integral

$$M_\nu \approx \int \mathrm{d}u u^\nu \int \mathrm{d}^3v f(\mathbf{v})\mathbf{v}\cdot\hat{n}\delta(u - \mathbf{v}\cdot\hat{n})\,. \tag{4}$$

Carrying out the integration over u,

$$M_\nu \approx \int \mathrm{d}^3v (\mathbf{v}\cdot\hat{n})^{\nu+1} f(\mathbf{v})\,. \tag{5}$$

* This assumption is valid for Mach number $\gtrsim 2$.

** In practice G must be corrected for the transparency of the grid structure but the variation of transparency with angle is small so that G is well represented as a constant less than unity.

© Kluwer Academic Publishers • Provided by the NASA Astrophysics Data System

1977SSRv...21..259B

Comparing this with the definitions of the plasma parameters, we see that (for simplicity the direction $\hat{n}$ is taken as the z axis):

$$M_{-1} = N;$$

$$M_0 = NV_z;$$

$$mM_1 = mNV_z^2 + P_{zz};$$

$$\tfrac{1}{2}mM_2 = \tfrac{1}{2}mNV_z^3 + \tfrac{3}{2}V_zP_{zz} + Q_{zzz}.$$

N is the ion number density, $\mathbf{V}$ the bulk velocity, $\mathbf{P}$ the pressure tensor, and $\mathbf{Q}$ the third rank tensor whose contraction is the heat flux vector $\mathbf{q}$:

$$Q_{ijk} \equiv \int \mathrm{d}^3v w_i w_j w_k f(\mathbf{v}), \qquad \mathbf{w} \equiv \mathbf{v} - \mathbf{V};$$

$$q_i \equiv \sum_j Q_{ijj}.$$

Thus, each collector provides measurements of (1) the ion number density, (2) the bulk velocity component along the normal to the collector, (3) the component of the pressure tensor along the normal, and (4) the component of the heat flux tensor along the normal. (In practice, to improve precision, the latter two are to be calculated not from M_1 and M_2 directly but from the corresponding central moments:

$$\sum_k \frac{I_k}{eA\,\Delta u_k}(u_k - V_z)^\nu \Delta u_k, \qquad \nu = 1, 2.$$

The complete set of measurements from the three collectors pointing in three different directions provides (1) three independent measurements of the density; (2) a measurement of the bulk velocity components along the three directions, and hence the complete bulk velocity vector; (3) a measurement of the pressure tensor components along the three directions, from which $P_\perp$ and $P_\parallel$ can be obtained with the use of the magnetic field direction measured by the magnetometer; (4) a measurement of the heat flux tensor Q components along the three directions; from this result the independent components $Q_\parallel$ and $Q_\perp$ and hence the parallel heat flux $q_\parallel = Q_\parallel + 5Q_\perp$ can be obtained as in case (3). (The assumption that the distribution function is axially symmetric about the magnetic field direction is expected to be very good in the solar wind: significant departures from it require variations on time scales shorter than a gyroperiod and/or spatial scales shorter than a gyroradius.)

The data afford several tests which can be used to ensure that the plasma lies within the primary field of view of the instrument. One check is the agreement of the three density measurements. Another is that the derived velocity vector lie within the primary field of view; it can easily be shown that if the true velocity lies outside it, the derived velocity will be even further outside. For the case that the plasma is only within the secondary field of view, the instrument is essentially equivalent to three

© Kluwer Academic Publishers • Provided by the NASA Astrophysics Data System

1977SSRv...21..259B

ordinary Faraday cups and the data can be analyzed by conventional model fitting techniques.

The accuracy of the estimated plasma parameters was studied by a computer simulation. A convected isotropic Maxwellian distribution with bulk speed near 400 km sec^{-1} was used to represent the incident solar wind. The number density was allowed to range from 3×10^{-3} to 10 protons cm^{-3}; the wind Mach number (bulk speed/most probable thermal speed) was varied from 1 to 100, and a Gaussian noise level current with $\sigma = 3\times10^{-14}$ amp (this is the expected noise level for the 930 millisec integration time) was randomly added to the currents calculated for each energy window. The rms percentage errors in bulk speed, number density, and thermal speed were computed for ten trials with randomly chosen values of bulk speed (to explore the full width of the energy channel containing the peak current). The results given in Table III are based on moments calculated from currents in the M or L modes. Some improvement in the values given in the table is attainable at high Mach numbers and low densities by using a model distribution function rather than the moment calculation alone.

TABLE III

Percent error in parameter estimate vs number density and Mach number (V = bulk speed, N = number density, W = most probable thermal speed)

Number density (cm^{-3})	Estimated parameter	Mach number 1	3	10	30	100
10	V	16	<0.1	<0.1	<0.1	<0.1
	N	13	<0.1	0.2	0.2	0.5
	W	21	0.2	0.3	2.5	27
1 (2.4 AU[a])	V	15	0.3	<0.1	<0.1	<0.1
	N	13	0.4	0.2	0.2	0.6
	W	20	1.6	0.4	2.7	26
0.1 (7.7 AU[a])	V	15	0.5	<0.1	<0.1	<0.1
	N	14	0.9	0.4	0.4	0.4
	W	22	2.7	1.2	3.4	31
0.01 (24 AU[a])	V	20	3.2	0.4	0.2	0.1
	N	23	6.8	3.0	2.4	2.8
	W	27	1.2	3.2	18	41
0.003 (44 AU[a])	V	48	6.5	1.9	0.3	0.3
	N	32	8.0	7.3	6.3	7.7
	W	35	13	69	26	131

[a] Note: Distance at which the number density represents the average solar wind conditions assuming a value of 6 cm^{-3} at 1 AU, and an inverse r^2 dependence on distance.

The response of the instrument to the corotating plasma in the Jovian magnetosphere was studied using the same technique. At $5R_j$, the bulk speed of the plasma in

© Kluwer Academic Publishers • Provided by the NASA Astrophysics Data System

1977SSRv...21..259B

the spacecraft frame is expected to be about 35 km sec^{-1}. The number density and thermal speed there have been measured to be ~20 cm^{-3} and ~140 km sec^{-1} (Frank *et al.*, 1976). The computer simulation indicates that, at a number density of 10 cm^{-3}, the experiment is capable of estimating accurately, using a model fitting procedure, the properties of a plasma with a bulk speed of 30 km sec^{-1} and thermal speed as low as 80 km sec^{-1}.

4. Scientific Objectives and Expected Results

4.1. Introduction

The Pioneer 10 and 11 missions have provided a wealth of information on the plasma environment of Jupiter and on the properties of the solar wind from 1 AU to distances well beyond 5 AU. As a result, the scientific objectives for the encounter and cruise phases of the Voyager mission are more sharply formulated and defined than was the case in 1972 when the instruments were proposed (see for example, Smith *et al.*, 1976; Acuña and Ness, 1976; Intriligator and Wolfe, 1976; Scarf, 1976; Gosling *et al.*, 1976; and references in those papers).

A primary goal of the Voyager plasma experiment is the large-scale mapping of the plasma populations and processes in the outer and inner regions of the Jovian magnetosphere and in the magnetotail. Even with the Pioneer 10 and 11 results, our knowledge of the general morphology of the plasma environment of Jupiter is still very incomplete. In particular, better and more complete information about the shape and position of the bow shock, magnetopause and other possible boundaries is badly needed. The extremely large variations in the locations of the magnetopause observed by the Pioneer experiments are, at present, without adequate explanation. We do know that variations in the dynamic pressure of the incident solar wind are much larger than had been believed (see Section 4.6 below) and this fact may provide at least a partial explanation of the observations. During the JST encounter with Jupiter, it should be possible to predict the dynamic pressure and the boundary positions as a function of time using results from the JSX experiment and from experiments in Earth orbit. The comparison of the predicted positions with those actually observed during the JST encounter may help resolve some of the questions posed by the Pioneer observations.

The electron measurements form an essential part of the large scale mapping of the magnetosphere and one principal result will be a map showing the spatial extent and physical characteristics of electron populations in the outer and inner magnetosphere. In at least part of the outer magnetosphere, convection should be driven by the external flow; in that case, plasma electrons should have energies of a few hundred to a few thousand volts corresponding to a solar wind (magnetosheath) source. The characteristics of the electrons will be especially useful in understanding the transition from the inner magnetosphere (dominated by corotation) to the distant magnetotail (which must result from the external flow).

© Kluwer Academic Publishers • Provided by the NASA Astrophysics Data System

1977SSRv...21..259B

In the following sections we outline the scientific objectives of the Voyager plasma experiment during various phases of the mission and summarize the expected results.

4.2. The Outer Jovian Magnetosphere and Magnetotail

Much of our present understanding of Jovian magnetospheric physics has been built up by analogies to the terrestrial case, even though the overall configurations of the two magnetospheres are rather different. In discussing the scientific objectives at Jupiter encounter it is, therefore, instructive to first review some basic physical processes in Earth's magnetosphere. (We follow the general approach outlined in Vasyliunas, 1975, 1976.) We then consider the Jovian magnetosphere, with emphasis on the similarities and intrinsic differences as compared to the magnetosphere of Earth.

Most activity in Earth's magnetosphere is related directly or indirectly to the process of magnetospheric convection. This process results from the 'freezing' of the plasma and magnetic field; that is, motion at one point on a magnetic field line implies motion on the entire line. There are important exceptions to freezing, but the concept is valid for large-scale systems. Magnetospheric convection is the circulation of magnetospheric plasma driven by tangential drag due to the external (magnetosheath) flow over the boundary of the magnetosphere, in a pattern schematically illustrated in Figure 5. The source of the tangential drag is the entry into the magnetosphere of external magnetosheath plasma which carries with it momentum

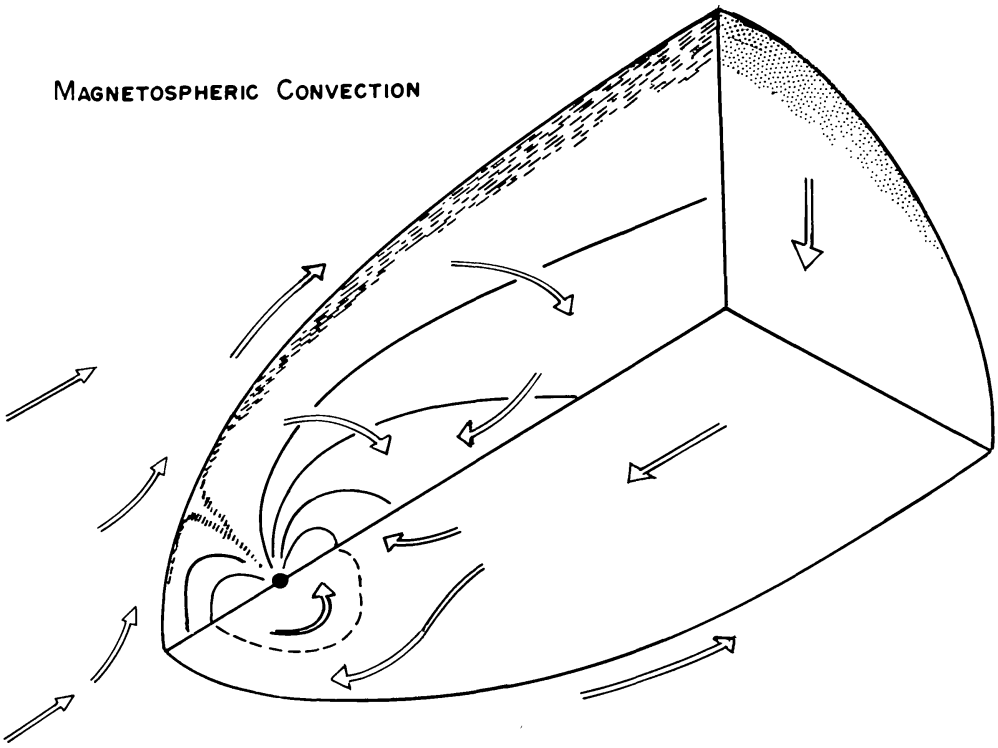

Fig. 5. Circulation patterns of magnetospheric convection in Earth's magnetosphere. The shaded region denotes the boundary layer formed by the entry of external plasma into the magnetosphere. (After Vasyliunas, 1976).

© Kluwer Academic Publishers • Provided by the NASA Astrophysics Data System

1977SSRv...21..259B

from the external flow. It forms a boundary layer (shaded in Figure 5), which is directly observed in Earth's magnetosphere.

Among the effects of magnetospheric convection are (1) the formation of a magnetotail due to the stretching of the magnetic field lines, thereby storing magnetic energy; (2) the compression and acceleration of plasma by the return flow, which produces auroral particles and serves as an input to the radiation belts; (3) the sweeping of plasma out of the outer magnetosphere in one circulation time, which is roughly the time it takes for the solar wind to flow over the magnetosphere; therefore, the plasma source in the outer magnetosphere is the solar wind and/or short-term accumulation (over less than one circulation time) of ions and electrons from the ionosphere and (4) the explosive release of energy (magnetospheric substorm) built up in the magnetotail by the nonsteady convection. All of these processes are associated with the drag exerted by the solar wind plasma as it flows over the boundary of the magnetosphere.

The rotation of the ionosphere also exerts a drag on the magnetospheric plasma. The effect of this ionospheric drag is to produce a corotating region near the planet (see Figure 6), within which long-term accumulation of plasma from the ionosphere

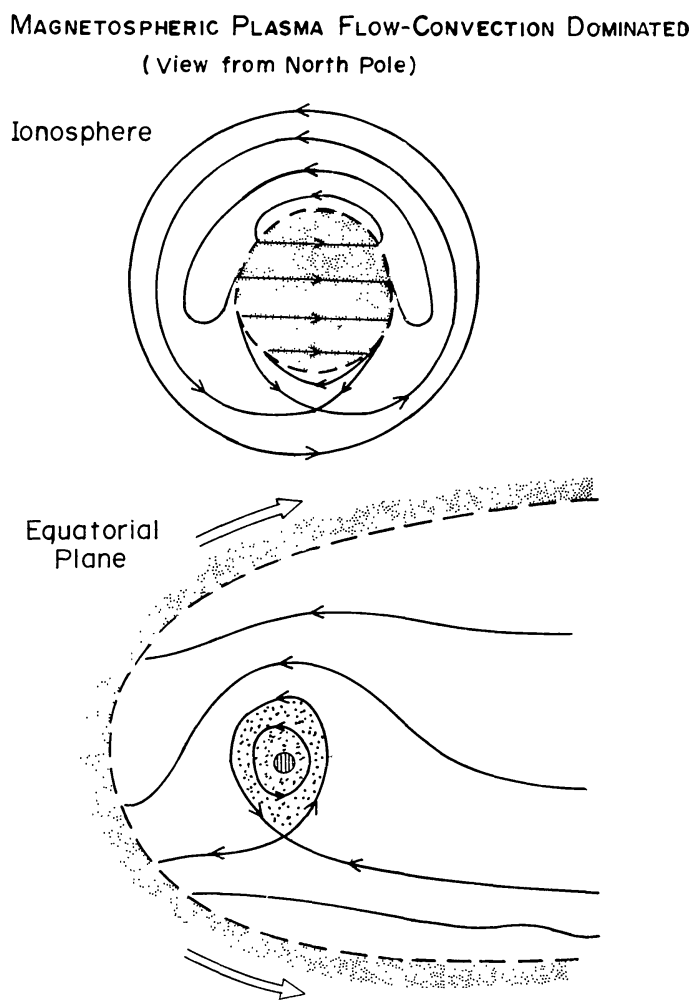

Fig. 6. Magnetospheric flow topology for the convection-dominated case. (After Vasyliunas, 1975.)

© Kluwer Academic Publishers • Provided by the NASA Astrophysics Data System

1977SSRv...21..259B

is possible. Because of the sweeping out of plasma due to magnetospheric convection, the extent of the corotating region is determined by the ratio of the solar wind flow time to the rotation period. If this ratio is small, magnetospheric convection can empty the outer magnetosphere many times in one rotation period, and the extent of the corotating region is small compared to the region of magnetospheric convection. This is the case for Earth, whose magnetospheric flow topology is convection-dominated (see Figure 6).

These concepts may also be applied to the case of the Jovian magnetosphere. The strong magnetic field of Jupiter implies a large magnetosphere and thus a long solar wind flow time over the magnetosphere. Coupled with the shorter rotation period, this implies that the ratio of solar wind flow time to rotation period is greater than one. Convection cannot empty the magnetosphere within one rotation, and the magnetospheric flow topology should be rotation-dominated (see Figure 7). The large extent of the corotation region is generally supported by the Pioneer 10 and 11

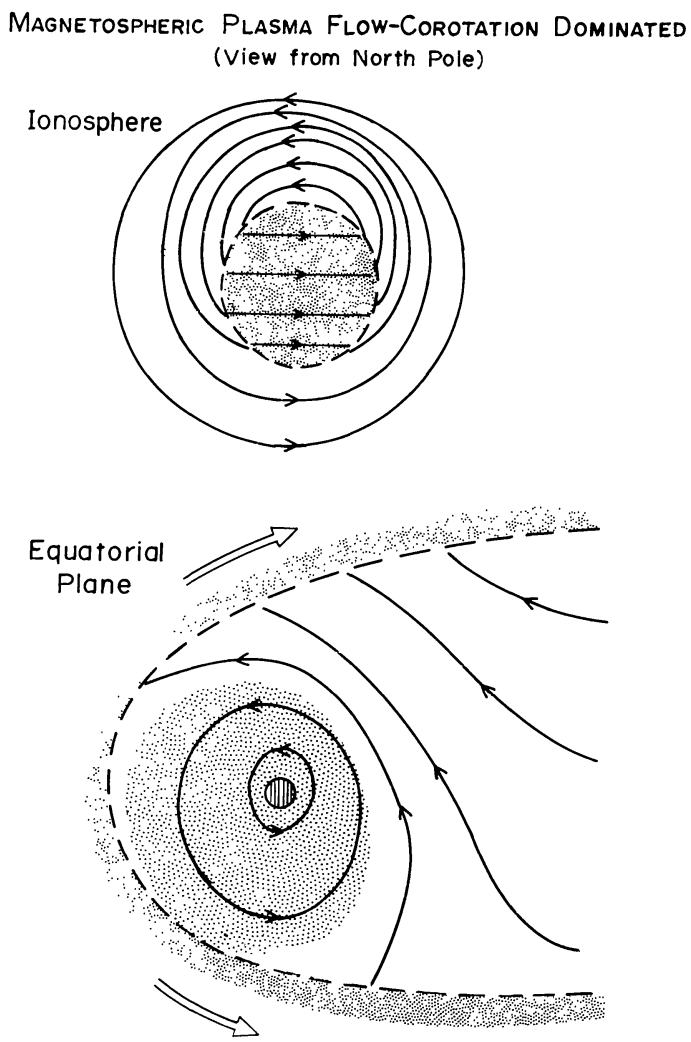

Fig. 7. Magnetospheric flow topology for the corotation-dominated case. (After Vasyliunas, 1975.)

© Kluwer Academic Publishers • Provided by the NASA Astrophysics Data System

1977SSRv...21..259B

results such as the centrifugal distortion of the magnetic field (Smith *et al.*, 1974) and an energetic particle anisotropy consistent with corotation out to some 60 R_J (Trainor *et al.*, 1974).

Because of this rotation-dominated topology, the boundary layer between the Jovian magnetosphere and the solar wind is expected to be very different from that of the Earth. Since the corotational speed at the boundary of the magnetosphere is larger than the solar wind speed, a useful approximation is to consider a nearly stationary external plasma surrounding a rotating magnetospheric plasma. If this is a valid representation of the Jovian situation, the field line stretching due to tangential drag may be azimuthal, rather than tailward as at Earth (the 'wrapped-around magnetotail' of Piddington, 1969 and Van Allen *et al.*, 1974). The observed B_ϕ in the outer magnetosphere (Smith *et al.*, 1974) is consistent with the existence of tangential drag. The effect of such a drag may lead to the existence of a region where external plasma can enter (shaded region in Figure 7).

An alternate view of the interaction is that the solar wind exerts confining pressure (to balance centrifugal stress) on the dayside, but not on the nightside. Therefore, as field lines rotate from day to nightside, they break off tailward. This concept and its various consequences have been explored in a series of papers by Dessler, Hill and their co-workers (see Hill and Dessler, 1976, and references therein). The process may be analogous to magnetospheric substorms, solar flares, and other explosive releases of magnetic energy. There are some effects of this process on the dayside: the plasma removed from flux tubes in the outer magnetosphere can only be that due to short-term refilling from the ionosphere in less than one rotation period.

Turning to the interpretation of the Voyager measurements, the observational signature of tangential drag is the existence of an internal boundary layer – magnetosheath plasma on magnetosphere field lines, and possibly also an external boundary layer (i.e., the adjacent magnetosheath flow may be affected by the drag, by virtue of Newton's third law; this effect is very small at Earth but may be large at Jupiter). The observational signatures of possible sources of plasma in the outermost magnetosphere are:

(1) For long-term accumulation from the ionosphere, there should be no flow parallel to the magnetic field, the mean energy should be related to the corotational energy and therefore should increase with increasing radial distance, and the particle density should be unrelated to that in the solar wind;

(2) For short-term accumulation, there should be a large parallel flow (the time to fill a flux tube is long compared to a rotation period), with a mean energy which increases with decreasing distance;

(3) For entry from the solar wind, we have again no parallel flow, a mean energy related to solar wind energy and increasing with decreasing distance (energy proportional to the magnetic field), and a density related to the solar wind density.

The plasma instrument has a broad sensitivity for the detection of plasma ions at Jupiter. We show in Figure 8 the expected particle populations at Jupiter with the

© Kluwer Academic Publishers • Provided by the NASA Astrophysics Data System

1977SSRv...21..259B

threshold of the Voyager instrument indicated. The sensitivity is adequate to observe particle populations which are much less intense than those seen by Pioneer 10.

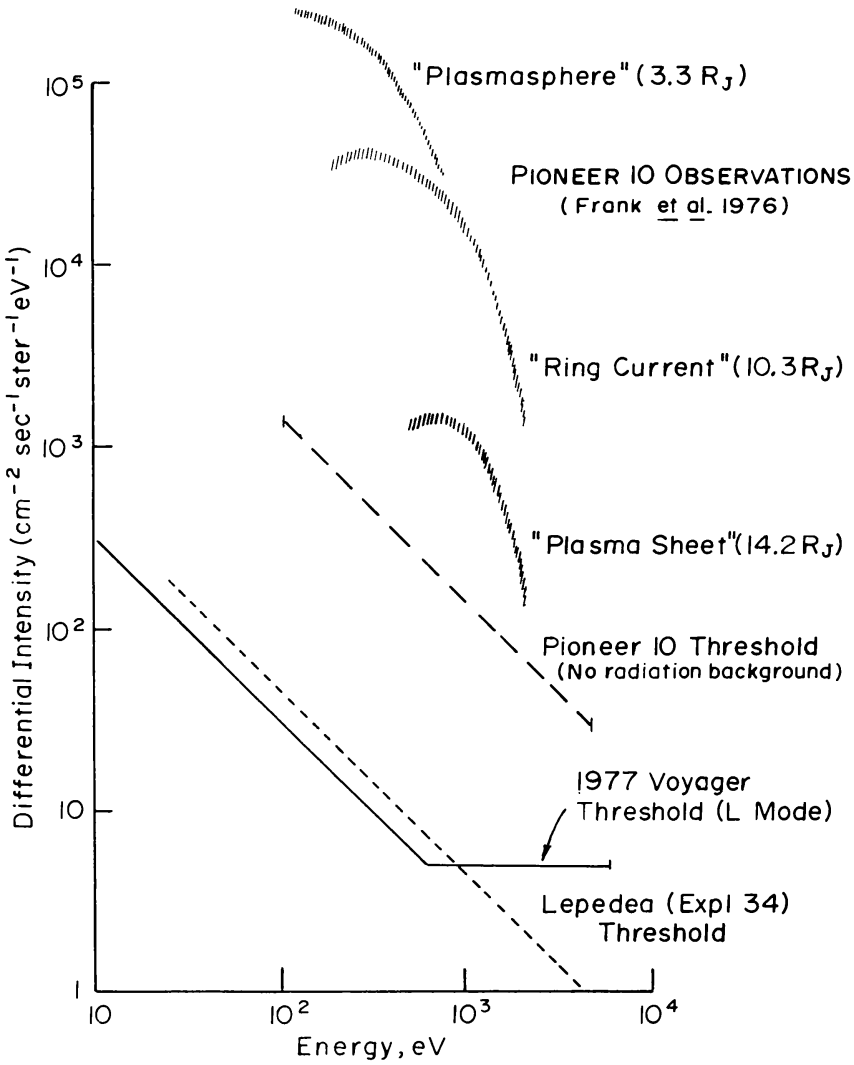

Fig. 8. The predicted sensitivity of the Voyager instrument in the Jovian environment compared with the sensitivity of some other instruments using intensities expected on the basis of the Pioneer 10 results.

4.3. The inner Jovian magnetosphere

The plasma contained within the inner magnetosphere of Jupiter is thought to originate from two principal sources. First, ions and electrons from the ionosphere diffuse along field lines in the combined gravitational and centrifugal potential to populate the plasmasphere (Ioannidis and Brice, 1971; Mendis and Axford, 1974; Hill and Michel, 1975); second, neutral particles escape from the atmospheres or surfaces of the inner satellites and become ionized by photons or by electron impact to form part of the observed plasma. A large amount of experimental and theoretical work has been done to identify the sources of the plasma, the loss mechanisms and the transport processes (see for example the review by Brown and Yung, 1976 and

© Kluwer Academic Publishers • Provided by the NASA Astrophysics Data System

1977SSRv...21..259B

references therein; and Siscoe, 1977a and 1977b). One of the principal experimental results expected from the Voyager flybys is a map of the ion and electron distributions (particle densities, energy spectra and intensities) in the inner magnetosphere. Such a map is also the goal of the theoretical efforts, and the experimental results should help to decide which of the present theories, if any, corresponds most closely to reality. In what follows we discuss some of the expected features of the inner magnetosphere in more detail.

(1) *Equatorial Confinement of Satellite Ions*: Io is known to be a source of neutral hydrogen, sodium and potassium atoms, which are confined for the most part to an incomplete torus centered on Io, with the axis of the torus coincident with the orbit of Io. The spread of the neutrals away from the axis, i.e., the radius of the torus relative to the axis, is about $1R_J$ (see the review by Brown and Yung, 1976, and references therein; Fang *et al.*, 1976). Ions from the neutral cloud are created near the orbital plane and the corotation of Jupiter's magnetic field gives a new ion a guiding center motion equal to, and a gyro-velocity comparable to, the corotation velocity. The resulting magnetic mirror and centrifugal forces maintain the equatorial confinement of the ions (Hill and Michel, 1975; Siscoe and Chen, 1976).

In addition to the observed neutral particle rings, there is an ionized cloud of sulfur which is associated with Io, most likely in the manner just described (Kupo *et al.*, 1976; Wehinger *et al.*, 1976). The cloud provides direct evidence for equatorial confinement. Its thickness relative to the orbital plane is also about $1R_J$. Finally, the ions in the inner plasmasphere discovered by the Pioneer 10 plasma experimenters (Frank *et al.*, 1976), if interpreted as originating from the Io neutral particle ring, also show strong equatorial confinement in their pitch angle behavior (Siscoe and Chen, 1976).

It is possible that other Galilean satellites also have neutral particle rings and consequently are sources of ions for the inner magnetosphere, although no emissions have yet been detected from the other satellites (e.g., Kupo *et al.*, 1976). There is, however, observational evidence for an atmosphere on Ganymede (Carlson *et al.*, 1973), and the presence of an atmosphere seems to imply necessarily the existence of a neutral particle ring (McDonough and Brice, 1973).

Ions created from the neutral particle rings will be carried to other regions in the magnetosphere, most likely by radial diffusion resulting from flux-tube interchange (see for example, Brice and McDonough, 1973; Coroniti, 1974, 1975; Siscoe and Chen, 1976). The spatial distribution and intensity of the ions expected under this assumption have been worked out in detail (Siscoe, 1977a). It turns out that ions from the ionosphere of Jupiter have different latitude distributions from those which originate from satellite surfaces or atmospheres because of their different pitch angle behaviour, and that ions from different Jovian satellites are themselves well separated in velocity space. Figure 9 shows the latitudinal regions to which ions from each of the inner satellites are confined, and Figure 10 shows, as an example, the regions in velocity space occupied by ions from the neutral particle rings of Io and Ganymede and from Jupiter's ionosphere at a distance of $20R_J$.

© Kluwer Academic Publishers • Provided by the NASA Astrophysics Data System

1977SSRv...21..259B

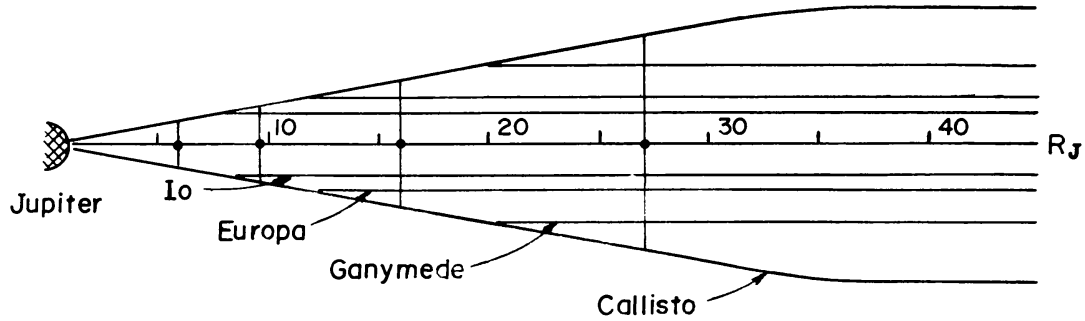

Fig. 9. The ion confinement discs corresponding to each of the Galilean satellites. The horizontal central line is the magnetic equator. The common flaring angle is 10° corresponding to the diurnal excursion of each satellite relative to the magnetic equator. The satellites, dots, and their diurnal excursions are indicated by the labeled vertical lines. The lower limit of the confinement disc of each satellite is also labeled by an arrow from the satellite's name.

Thus, at any distance from Jupiter, the ions from each given satellite occupy a specific and characteristic region in velocity space which varies as a function of radial distance in a predictable way. In favorable cases the energy per charge distribution of the particle intensity (which is the fundamental observable for this instrument) and its variation with latitude and longitude can uniquely determine the charge to mass ratio(s) of the ions and the satellite(s) from which they come. The ion number density observed at the orbit of Io by Pioneer 10 was about 50 cm^{-3} (Frank *et al.*, 1976 as interpreted by Siscoe and Chen, 1976, and Neugebauer and Eviatar, 1976). If these ions originate at Io, the observed density can be extrapolated outward under the assumption of interchange diffusion; with corotating flow, their predicted intensity is more than two orders of magnitude above the threshold sensitivity of the instrument throughout the inner magnetosphere out to about $50R_J$.

4.4. The Io Flux Tube

During the JST encounter there is an opportunity to pass below Io through the flux tube which links Io and Jupiter. Observations of charged particles, waves and magnetic fields in the vicinity of the flux tube are of great interest not only because they bear directly on various explanations of the Jovian decametric radiation (see the review by Smith, 1976, and references therein) but also because the motion of the flux tube relative to the ambient plasma may have significant effects on the configuration of the magnetosphere (Piddington, 1969).

It is convenient to group the various models of the interaction into those that involve electrical currents linking Io and the ionosphere of Jupiter and those that do not. The first group contains the various unipolar induction models differing mainly in the details of the current closure at Io, for example, through the solid body (Goldreich and Lynden-Bell, 1969), through the ionosphere (Webster *et al.*, 1972), through plasma sheaths (Gurnett, 1972; Shawhan *et al.*, 1973) or through some combination of these. Other models which attempt to explain the effect of Io on the

© Kluwer Academic Publishers • Provided by the NASA Astrophysics Data System

1977SSRv...21..259B

decametric radiation without assuming unipolar induction have been proposed (Wu, 1973; Mendis and Axford, 1974). The theories predict different specific properties of the plasma in and near the flux tube which depend on the unknown values of the conductivities at each end of the tube. Thus, the specific behavior of the plasma in and near the flux tube is unknown at this time. However, it is clear that, if the unipolar induction mechanism is generally correct, the theories require that changes in the flow speed, flow direction, temperature and density will occur in and near the flux

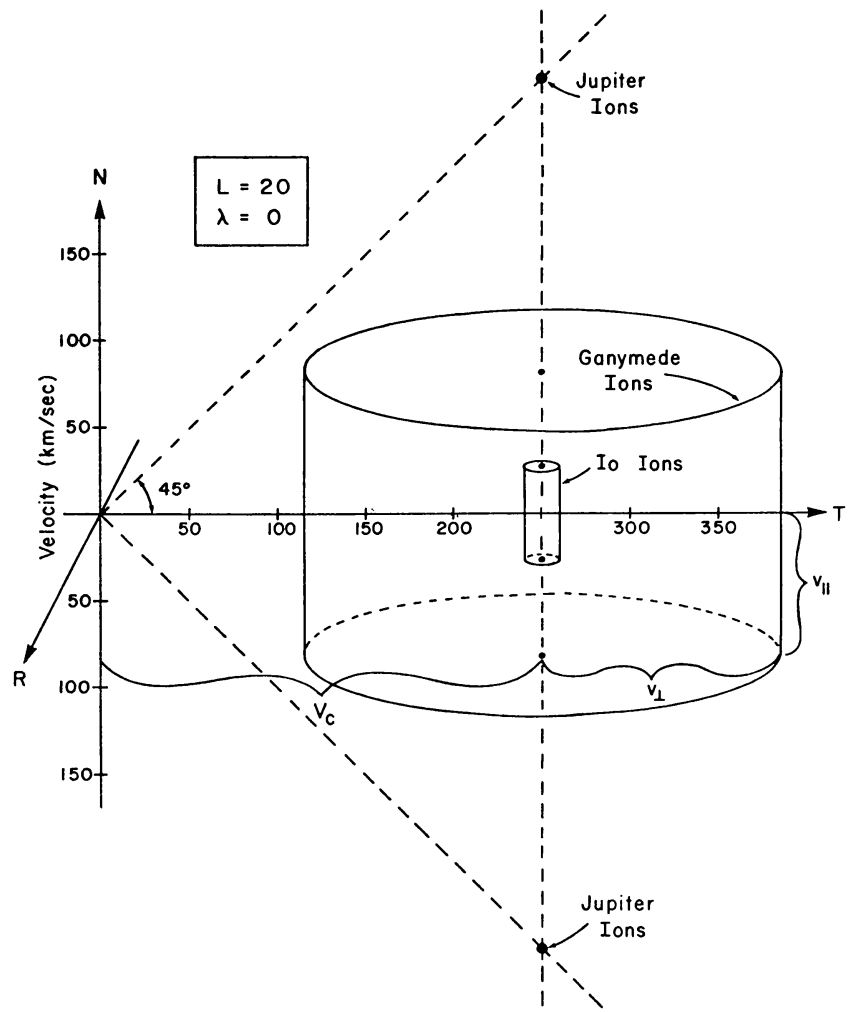

Fig. 10. The regions in velocity space occupied by ions from the neutral particle rings of Io and Ganymede and from Jupiter's ionosphere. The spatial location of the example is at a Jovicentric distance of $20R_J$ and in the magnetic equatorial plane. The axes are: V_R, the radial (from planet) velocity component; V_T, the velocity component in the direction of corotation; and V_N, the northward velocity component. In this case the V_N direction is parallel to the magnetic field (ignoring the 10° tilt).

tube; these changes in plasma properties should be observable by the present instrument. Some other theories predict that beams of energetic particles are produced at Io. These may or may not be observable by the plasma detector depending on the energies, directional properties and intensities of the particles.

© Kluwer Academic Publishers • Provided by the NASA Astrophysics Data System

1977SSRv...21..259B

4.5. Interaction of the solar wind with Saturn and Titan

Recent observations of non-thermal radio emission from Saturn (Brown, 1975) indicate that the magnetic field at the surface is of the order of one or two gauss. Thus, it is almost certain that Saturn has a magnetosphere, and the determination of its general configuration and properties is a primary objective during Saturn encounter. It will be especially interesting to compare the Saturnian magnetosphere with those of Mercury, Earth and Jupiter and to search for effects caused by the rings, e.g., absorption of charged particles.

The strength of the magnetic field inferred from the radio measurements implies that the stagnation point of the Saturnian magnetosphere lies in the range 20 to $40R_S$; thus (depending on the real value of the field and on solar wind conditions) the dayside orbit of Titan may lie inside or outside the magnetosphere. Therefore, the TB (Titan before Saturn) encounters which take place sunward of Saturn provide an opportunity to study the interaction between Titan and either the corotating magnetospheric plasma or the solar wind. If Titan has no intrinsic magnetic field, one expects a direct interaction between the atmosphere and the ambient plasma. The geometry of the TB encounters is such that wake phenomena characteristic of either interaction can be observed.

4.6. Measurements of the solar wind in the outer solar system

The present interpretation of the Pioneer 10 and 11 solar wind data (Lazarus, 1975; Hundhausen and Gosling, 1976) differs dramatically from earlier pictures of nearly steady, structureless flow beyond 1 AU. Nearly all of the solar wind streams observed at large heliocentric distances begin with abrupt jumps in the flow speed that are probably the shock fronts expected in the simplest concept of the nonlinear evolution of solar wind streams (Hundhausen, 1973a, 1973b). In fact, if solar wind observations made at 1 AU are used as boundary conditions in a quantitative model of this evolution, the predicted speed variations at 4–5 AU agree remarkably well with those actually observed by Pioneer 10 (Gosling *et al.*, 1976).

This view of stream evolution has important implications for the nature of the solar wind in the outer solar system, its interaction with galactic cosmic rays and the outer planets, and its ultimate merging into the interstellar medium. The steepening into shock waves between 1 and 5 AU, calculated on the basis of the actual solar wind data obtained at 1 AU is so drastic that nearly all ($\simeq$90–95%) of the plasma and magnetic field that flows past 1 AU is expected to pass 5 AU in thin compressed shells (2–3 days long) with the remaining amounts (5–10%) passing 5 AU in broad rarefaction regions (as much as 20 days long). Correspondingly, the microscale waves and turbulence in the solar wind should display anomalously high levels in the compression regions and relatively low levels in the rarefaction regions. Thus, the large scale variations in density and magnetic field strength are expected to become more pronounced as the plasma propagates from 1 to 5 AU.

Only a few observations of plasma density and temperature from Pioneer 10 and 11 are available to check these predictions; however, the magnetic field intensity and

© Kluwer Academic Publishers • Provided by the NASA Astrophysics Data System

1977SSRv...21..259B

microscale fluctuation levels observed by Smith on Pioneer 10 (Smith and Wolfe, 1976) evidently follow a pattern similar to that described above. Extension of the quantitative model of stream steepening to 20 AU predicts continued growth of these 'induced' density and magnetic field structures. At this latter distance, the density and magnetic field are predicted to vary by more than two orders of magnitude, and the proton temperature is expected to change from a few hundred degrees in rarefactions to a few times 10^5 K behind shock fronts.

We are thus led to the strong possibility (apparently confirmed between 1 and 5 AU) that the solar wind becomes increasingly inhomogeneous as it flows through the outer solar system. If this is the case, galactic cosmic rays enter the solar system along magnetic field lines that become confined to a small fraction of a heliocentric sphere near 5–10 AU; the magnetospheres of outer planets are immersed in a plasma flow where the momentum flux changes abruptly by one or two orders of magnitude, and the flow into the interstellar medium contains a series of shock waves with corresponding variations in the particle density and magnetic field. Especially at large heliocentric distances these predictions differ greatly from those based on a uniform coronal expansion and structureless solar wind (Parker, 1963). Some pertinent results expected from the Voyager plasma observations in the interplanetary medium are the following:

(1) A complete mapping of these large scale vector velocity and density variations to distances beyond 20 AU;

(2) Measurements, in the compression regions, of proton temperature perpendicular and parallel to the magnetic field, proton heat flux, and MHD wave amplitudes to distances beyond 20 AU;

(3) Measurements, in the rarefaction regions, of proton temperature, heat flux, and wave amplitude levels to 10–15 AU.

Such measurements are of great interest in themselves (e.g., nonlinear MHD stream evolution, the possibility of Alfvén wave survival over tens of AU, and so on). When combined with energetic particle measurements, they are invaluable to an understanding of cosmic ray diffusion in a turbulent and structured medium. The qualification as to radial extent in (3) above arises because of the more rapid fall-off of temperature in the rarefaction regions. However, predictions of such a fall-off do not consider possible heating due to thermalization of interstellar ions (see below). If such heating occurs, proton temperatures in rarefaction regions probably will *not* fall below observable levels at any radial distance (Semar, 1970; Holzer, 1972). The rate of heating with distance gives an indirect measure of the interstellar neutral hydrogen densities; the optimal region to look for such heating is in the rarefaction regions.

Theoretical models of the interaction of the solar wind with the interstellar medium (see Axford, 1973, and references therein) indicate a reasonable possibility of encountering the subsonic transition of the solar wind during an extended Voyager mission. The transition might be continuous but is more likely a shock wave. Even in the case of a shock transition, sunward of the shock the solar wind will gradually be slowed and possibly heat by the pick-up of ions from the ionization of the interstellar neutral hydrogen. The location of the transition is also related to the interstellar

© Kluwer Academic Publishers • Provided by the NASA Astrophysics Data System

1977SSRv...21..259B

hydrogen density and its speed relative to the Sun. Beyond the transition, the subsonic flow will be deflected by the interaction with the interstellar gas; the sense of the deflection is away from the stagnation region where the solar wind runs directly into the streaming neutral gas. The sense of deflection then gives an indication of the direction of motion of the interstellar gas. In the vicinity of the shock (if it exists) one expects to see multiple shock encounters as the shock moves in and out in response to variations in solar wind parameters. The radial distance over which this is expected to occur is the characteristic scale of large-scale solar wind variations, approximately 2–3 AU or greater.

4.7. The characteristics and detection of ions from the interstellar neutral hydrogen

The above comments on heating associated with interstellar material assume immediate thermalization of the ions created by charge exchange and photoionization of the neutrals. At present, the rate at which thermalization of these ions proceeds is unknown. If there is no thermalization, then the protons resulting from ionization of interstellar hydrogen can be distinguished from the solar wind protons through their different distributions in velocity space. Newly created ions have a speed perpendicular to B approximately equal to the local solar wind flow speed. The particles are then adiabatically decelerated as they move outward into weaker magnetic fields; their initially flat pitch angle distribution may be modified by various mechanisms, e.g., magnetic field fluctuations or instabilities driven by the pitch angle anisotropy, and may tend toward isotropy. Although the details cannot be predicted with any certainty, it is sufficient, for the purpose of separating interstellar from solar wind ions, to note that the interstellar ions will lie on a sphere in velocity space, centered on the point representing the solar wind flow velocity and with a characteristic radius equal to the flow speed. The solar wind ions are also distributed nearly spherically around the solar wind velocity, but with a characteristic radius equal to the much smaller solar wind thermal speed. More detailed calculations of the expected spectra of interstellar ions, as well as their intensity and its variation with heliocentric distance have been published elsewhere (Vasyliunas and Siscoe, 1976, and references therein).

The intensity of ions resulting from the ionization of interstellar neutral hydrogen is predicted to reach a maximum at a distance that depends on the neutral hydrogen density and on the speed and direction (relative to the point of observation) of the Sun's motion through the interstellar gas. For example, if the neutral hydrogen density is 0.1 cm^{-3} (the approximate upper limit set by Lyman alpha measurements) and if the streaming speed of the gas relative to the Sun is 10 km sec^{-1} (a commonly used value), then in the direction of the Sun's motion, the maximum intensity of 5.3×10^4 cm^{-2} sec^{-1} will occur at 13 AU. The peak is very broad and decreases by a factor of only 2 over the radial range 3.5 AU to 75 AU. It should be noted that the interstellar ion intensity should become detectable at a radial distance much less than that where appreciable effects of the direct interaction with the interstellar medium

© Kluwer Academic Publishers • Provided by the NASA Astrophysics Data System

1977SSRv...21..259B

become evident in the observed properties of the solar wind. With the wide energy-angle windows of the low resolution mode of the Voyager instrument, one-fifth to one-third of the volume in velocity space occupied by the interstellar ions can be measured. In this mode the instrument is capable of detecting the interstellar ions (in spite of their low velocity space density) over a wide radial range, particularly if there is little thermalization.

5. Scientific and Engineering Staff

The group of scientific investigators and engineers responsible for the design and construction of the Voyager plasma experiment and for the analysis of the data are as follows:

Massachusets Institute of Technology
H. S. Bridge – Principal Investigator
J. W. Belcher – Co-Investigator
A. J. Lazarus – Co-Investigator
S. Olbert – Co-Investigator
J. D. Sullivan – Co-Investigator

Goodard Space Flight Center
L. F. Burlaga – Co-Investigator
R. E. Hartle – Co-Investigator
K. W. Ogilvie – Co-Investigator

High Altitude Observatory
A. J. Hundhausen – Co-Investigator

Jet Propulsion Laboratory
C. M. Yeates – Co-Investigator

Max-Planck-Institut für Aeronomie, Katlenburg-Lindau
V. M. Vasyliunas – Co-Investigator

University of California, Los Angeles
G. L. Siscoe – Co-Investigator

The instrument has been designed and constructed at MIT's Laboratory for Space Experiments under the general direction of Dr J. H. Binsack. The engineering group is headed by R. J. Butler; Dr A. Mavretic, P. Bosshart, J. Davin, R. Steendal, R. Burgess and D. Galvin were responsible for most of the design and testing of the experiment. Dr E. F. Lyon made major contributions to the design, most notably to the modulator and the radiation shielding. Finally, though it is impossible to acknowledge properly the unstinting cooperation and assistance of our colleagues at JPL, we wish to give our special thanks to Henry Mertz, who represented this

© Kluwer Academic Publishers • Provided by the NASA Astrophysics Data System

1977SSRv...21..259B

experiment in its engineering aspects, and to Dr E. Franzgrote, who filled a similar role regarding scientific liaison.

References

Acuña, M. H. and Ness N. F.: 1976, in T. Gehrels (ed.), *Jupiter*, University of Arizona Press, Tucson, Arizona, p. 830.
Axford, W. I.: 1973, *Space Sci. Rev.* **14**, 582.
Brice, N. M. and McDonough, T. R.: 1973, *Icarus* **18**, 206.
Bridge, H. S., Dilworth, C., Rossi, B., Scherb, F., and Lyon, E. F.: 1960, *J. Geophys. Res.* **65**, 3053.
Bridge, H. S., and Vasyliunas, V. M.: 1973, *EOS Trans. AGU*, **54**, 440.
Brown, L. W.: 1975, *Astrophys. J.* **198**, L89.
Brown, R. A. and Yung, Y. L.: 1976, in T. Gehrels (ed.), *Jupiter*, University of Arizona Press, Tucson, Arizona, p. 1102.
Carlson, R. W., Bhattacharyga, J. C., Smith, B. A., Johnson, T. V., Hidayat, B., Smith, S. A., Taylor, G. E., O'Leary, B. T., and Brinkmann, R. T.: 1973, *Science* **182**, 53.
Collard, H. R. and Wolfe, J. H.: 1974, in C. T. Russell (ed.), *Solar Wind Three*, Institute of Geophysics and Planetary Physics, University of California, Los Angeles.
Coroniti, F. V.: 1974, *Astrophys. J. Suppl.* **27**, 261.
Coroniti, F. V.: 1975, in V. Formisano (ed.), *The Magnetospheres of the Earth and Jupiter*, D. Reidel Publishing Co., p. 391.
Fang, T.-M., Smyth, W. H., and McElroy, M. B.: 1976, *Planet. Space Sci.* **24**, 577.
Frank, L. A., Ackerson, K. L., Wolfe, J. H., and Mihalov, J. D.: *J. Geophys. Res.* **81**, 457.
Goldreich, P. and Lynden-Bell, D.: 1969, *Astrophys. J.* **156**, 59.
Gosling, J. T., Hundhausen, A. J., and Bame S. J.: 1976, *J. Geophys. Res.* **81**, 2111.
Gurnett, D. A.: 1972, *Astrophys. J.* **175**, 525.
Hill, T. W. and Michel, F. C.: 1975, *Rev. Geophys. Space Phys.* **13**, 967.
Hill, T. W. and Dessler, A. J.: 1976, *J. Geophys. Res.* **81**, 3383.
Holzer, T. E.: 1972, *J. Geophys. Res.* **77**, 5407.
Hundhausen, A. J.: 1973a, *J. Geophys. Res.* **78**, 1528.
Hundhausen, A. J.: 1973b, *J. Geophys. Res.* **78**, 2035.
Hundhausen, A. J. and Gosling, J. T.: 1976, *J. Geophys. Res.* **81**, 1436.
Intriligator, D. S. and Wolfe, J. H.: 1976, in T. Gehrels (ed.), *Jupiter*, University of Arizona Press, Tucson, Arizona, p. 848.
Ioannidis, G. and Brice, N. M.: 1971, *Icarus* **14**, 360.
Kupo, I., Mekler, Y., and Eviatar, A.: 1976, *Astrophys. J.* **205**, L51.
Lazarus, A. J.: 1975, *EOS Trans AGU*, **56**, 438.
McDonough, T. R. and Brice, N. M.: 1973, *Icarus* **20**, 136.
Mendis, D. A. and Axford, W. I.: 1974, *Ann. Rev. Earth Planet. Sci.* **2**, 419.
Neugebauer, M. and Eviatar, A.: 1976, *Geophys. Res. Lett.* **3**, 708.
Parker, E. N.: 1963, in *Interplanetary Dynamical Processes*, John Wiley and Sons, New York, chapters 9 and 10.
Piddington, J. H.: 1969, in *Cosmic Electrodynamics*, John Wiley and Sons, New York, p. 197.
Semar, C. L.: 1970, *J. Geophys. Res.* **75**, 6892.
Scarf, F. L.: 1976, in T. Gehrels (ed.), *Jupiter*, University of Arizona Press, Tucson, Arizona, p. 870.
Shawhan, S. D., Hubbard, R. F., Joyce, G., and Gurnett, D. A.: 1973, in R. Grard (ed.), *Photon and Particle Interactions with Surfaces in Space*, D. Reidel, Dordrecht, p. 405.
Siscoe, G. L. and Chen, C. K.: 1977, *Icarus* **31**, 1.
Siscoe, G. L.: 1977a, *J. Geophys. Res.* **82**, 1641.
Siscoe, G. L.: 1977b, Paper prepared for the NAS sub-panel on Heliosphere Hydromagnetics, Jan. 1977.
Smith, E. J., Davis, L., Jr., Jones, D. E., Coleman, P. J., Jr., Colburn, D. S., Dyal, P., Sonett, C. P., and Frandsen, A. M. A.: 1974, *J. Geophys. Res.* **79**, 3501.
Smith, E. J. and Wolfe, J. H.: 1976, *Geophys. Res. Lett.* **3**, 137.

© Kluwer Academic Publishers • Provided by the NASA Astrophysics Data System

1977SSRv...21..259B

Smith, E. J., Davis, L., Jr., and Jones, D. E.: 1976, in T. Gehrels (ed.), *Jupiter*, University of Arizona Press, Tucson, Arizona, p. 788.

Trainor, J. H., McDonald, F. B., Geegarden, B. J., Webber, W. R., and Roelof, E. C.: 1974, *J. Geophys. Res.* **79**, 3600.

Van Allen, J. A., Baker, D. N., Randall, B. A., Thomsen, M. F., Sentman, D. D., and Flint, H. R.: 1974, *Science* **183**, 309.

Vasyliunas, V. M.: 1971, in R. H. Lovbergs (ed.), *Methods of Experimental Physics*, Vol. 9B of *Plasma Physics*, Academic Press, p. 49.

Vasyliunas, V. M.: 1975, in V. Formisano (ed.), *The Magnetospheres of Earth and Jupiter*, D. Reidel Publishing Co., Dordrecht, Holland, p. 179.

Vasyliunas, V. M.: 1976, in B. M. McCormac (ed.), *Magnetospheric Particles and Fields*, D. Reidel Publishing Co., Dordrecht, Holland, p. 99.

Vasyliunas, V. M. and Siscoe, G. L.: 1976, *J. Geophys. Res.* **81**, 1247.

Webster, D. L., Alksne, A. Y., and Whitten, R. C.: 1972, *Astrophys. J.* **174**, 685.

Wehinger, P. A., Wyckoff, S., and Frohlich, A.: 1976, *Icarus*, **27**, 425.

Wu, C. S.: 1973, *Astrophys. J.* **186**, 313.

© Kluwer Academic Publishers • Provided by the NASA Astrophysics Data System